Electronic Supplementary Material (ESI) for Physical Chemistry Chemical Physics.

Supplemental Material: Interfacial Charge Transfer Enhancement via Formation of Binary Molecular Assemblies on Electronically Corrugated Boron Nitride

A.Tan, P. P. Zhang*

Department of Physics and Astronomy, Michigan State University, East Lansing, Michigan 48824-2320, USA

*corresponding author: zhang@pa.msu.edu

Section 1. Growth of ZnPc and F_{16}ZnPc Organic Assemblies

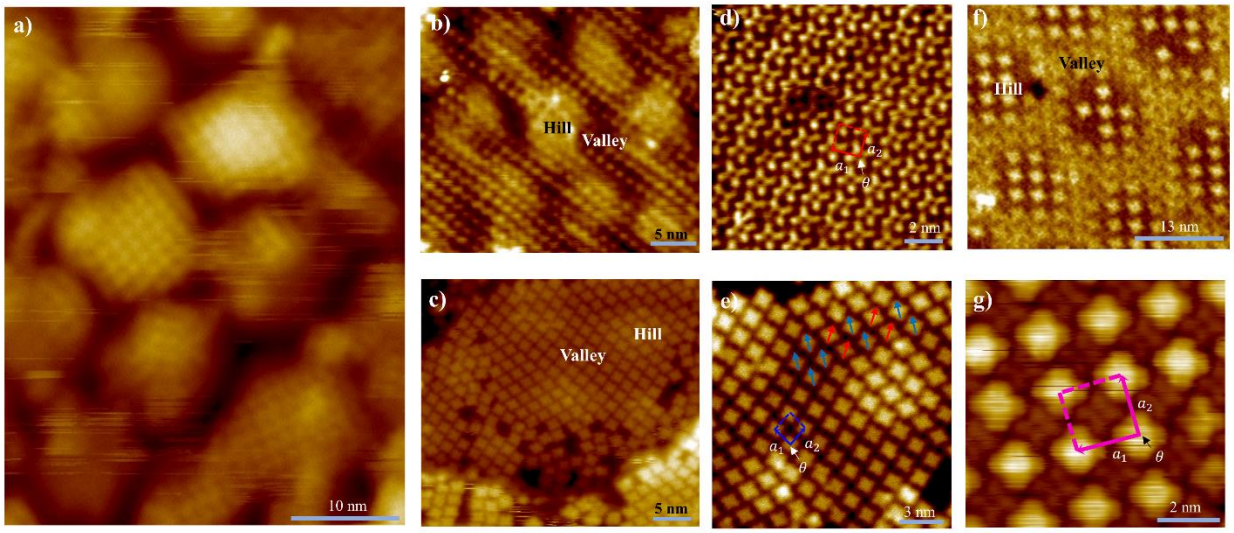

Figure S1: (a) STM topography images taken on ZnPc assembly at low coverage (V_s = 4 V, I_t = 1 pA) demonstrating nucleation preference of the molecules on h-BN hill locations. STM topography images taken on (b) ZnPc (V_s = 4 V, I_t = 2 pA) and (c) F_{16}ZnPc (V_s = 2 V, I_t = 1 pA) assemblies on h-BN/Cu(111), where the electronic perturbations of the h-BN Moiré patterns are observed. Zoomed-in STM topography images of (d) ZnPc (V_s = -1 V, I_t = 5 pA) and (e) F_{16}ZnPc (V_s = 2 V, I_t = 2 pA) showing the flower-petal structure of the Pc molecules and their orientation within the molecular layer. The F_{16}ZnPc overlayer on h-BN/Cu(111) proves to be less ordered with defects and vacancies more readily formed, along with the coexistence of two different azimuthal molecular orientations termed as α- and β-orientations and denoted by the blue and red arrows, respectively. The alternative molecular orientations can help minimize the repulsive interaction between the fluorine groups of adjacent F_{16}ZnPc molecules, as has been reported in

F_{16}CuPc assemblies formed on various substrates including Cu(111) and HOPG.[1-4] (f) STM topography image (V_s = 2 V, I_t = 1 pA) taken on the ZnPc/F_{16}ZnPc binary molecular superstructure, showing the periodic electrostatic modulation from the underlying h-BN/Cu(111) Moiré pattern. Bright molecules correspond to F_{16}ZnPc. (g) Zoomed-in STM topography image (V_s = 4 V, I_t = 10 pA) of the binary blend showing the flower-petal structure of ZnPc and F_{16}ZnPc molecules and their orientation within the molecular layer. The unit cells of the molecular overlayers are labeled in (d), (e) and (g), with the lattice parameters listed in Table S1.

Section 2. Electronic Perturbation of h-BN Moiré Pattern on Organic Assemblies

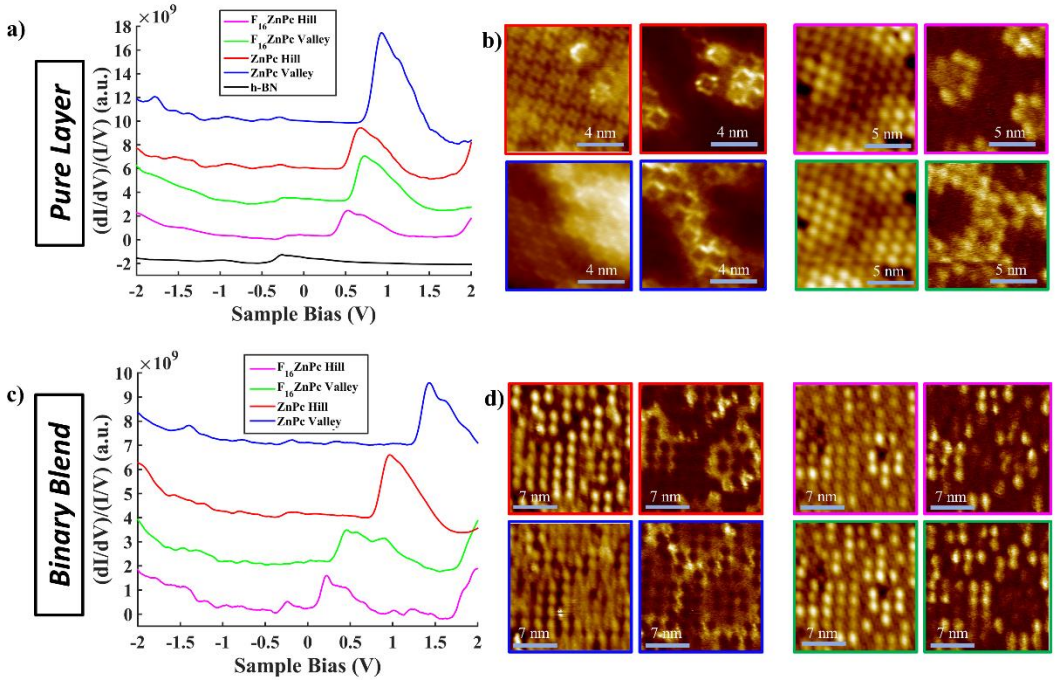

Figure S2: (a) STS data taken on h-BN/Cu(111) (setpoint: V_s = 2 V, I_t = 100 pA), and on the ZnPc (V_s = 2 V, I_t = 100 pA) and F_{16}ZnPc (V_s = 2 V, I_t = 50 pA) assemblies above the hill and valley locations within the Moiré patterns of the h-BN/Cu(111) substrate. The curves are vertically offset for clarity. As shown in (a), the STS curve (black) taken on h-BN/Cu(111) displays only a small step function arising from the electron tunneling directly between the tip and the Cu(111) surface state at ~-0.4 V.[5, 6] Simultaneously taken STM topography images (left columns) and dI/dV differential conductance maps (right columns) on (b) the ZnPc molecular overlayer (I_t = 100 pA) at V_s = 0.6 V (top, red frames) and V_s = 0.9V (bottom, blue frames) and the F_{16}ZnPc molecular overlayer (I_t = 30 pA) at V_s = 0.4 V (top, pink frames) and V_s = 0.6 V (bottom, green frames), corresponding to the LUMO peak levels of the individual molecular layers above the hill and valley locations of the Moiré pattern, respectively. (c) STS data (setpoint: V_s = 2 V, I_t = 100 pA) of the two molecular constituents in the ZnPc/F_{16}ZnPc binary blend on various Moiré locations. The curves are vertically offset for clarity. (d) Simultaneously taken STM topography images and dI/dV maps (I_t = 30 pA) on the ZnPc/F_{16}ZnPc binary superstructure, at V_s = 0.1 V, corresponding to the LUMO peak of F_{16}ZnPc at Moiré hills (top, pink frames), at V_s = 0.3 V, corresponding to the F_{16}ZnPc peak at Moiré valleys (bottom, green frames), at V_s = 1 V, corresponding to the ZnPc peak at Moiré hills (top, red frames), and at V_s = 1.2 V, corresponding to the ZnPc peak at Moiré valleys (bottom, blue frames).

Section 3. Gaussian Fits

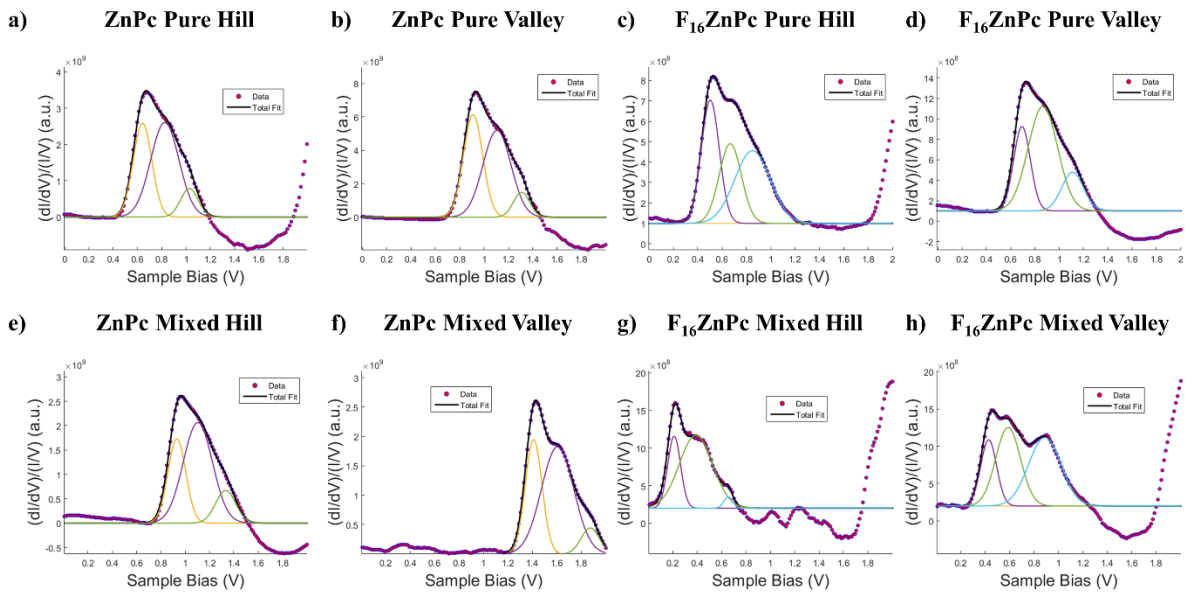

Figure S3: Gaussian Peak fitting of the (a, b) pure ZnPc spectrum, (c, d) pure F_{16}ZnPc spectrum, (e, f) binary mixed layer ZnPc spectrum and (g, h) mixed layer F_{16}ZnPc spectrum, was done using the fitting function in MATLAB. The spectra used here are reproduced from Fig. S2a, c for the pure and mixed layers, respectively. The first peak of the fitting is attributed to the molecular LUMO. Satellite peaks that lie at higher energies are associated with vibrational modes of Pc molecules. The average spacing between adjacent Gaussian peaks across all spectra is determined to be 0.21 ± 0.02 eV. ZnPc and F_{16}ZnPc spectra are combined for the purpose of this average due to the similarity between the vibrational energies of these molecules, particularly with regards to the relevant energy range.[7, 8] To accurately determine the vibrational energy in the presence of the h-BN layer, it requires the consideration of the voltage drop over the molecule leading to a corrected energy spacing of $(V_{vib})_{corr} = (1 - \alpha)V_{vib}$ where α = 0.093.[9] The actual energy spacing is therefore 0.19 ± 0.02 eV. The likely vibrational mode associated with this energy is the C=N aza + C=C pyrrole + C=C benzene mode which corresponds to 1528 cm^{-1} or 0.189 eV.[10]

Section 4. Polarization of Organic Molecules

When introducing a different molecular species into the matrix of a thin film, the polarizability of the different organic molecules can result in the change in the local electrostatic environment.[11-13] From a purely electrostatic consideration, barring changes to the molecule-substrate interaction and additional molecule-molecule interaction, the contribution of molecular polarization to the screening of excess charges (such as those created in an electronic structure measurement technique like STS) can be calculated using the following equation[11]:

$$E_{polarization} = \frac{Ne^2\alpha}{2R^4}$$

Where N is the number of closest molecular neighbors, α the polarizability of the molecular species, and R the intermolecular distance. Using the dielectric constant of the two molecular species as an appropriate analogue for the purpose of this calculation, we find that the contribution of the molecular polarization to the electrostatic screening is roughly equivalent in the pure molecular layers. The higher dielectric constant of F_{16}ZnPc (4.8) compared to ZnPc (4) is offset by the slightly larger unit cell that is adopted in the F_{16}ZnPc assembly.[1, 14] When considering the binary molecular superstructure, F_{16}ZnPc molecules are surrounded by ZnPc molecules and vice versa. The overall change in the screening effect results in a ~7% increase in polarization energy for ZnPc molecules and a ~10% decrease for F_{16}ZnPc molecules. This suggests that the LUMO of ZnPc molecules, upon formation of the binary superstructure, should shift towards the Fermi level while the LUMO of F_{16}ZnPc molecules should shift away from the Fermi level. This back-of-envelope calculation therefore suggests that our experimental observation is not the result of the different polarizabilities of ZnPc and F_{16}ZnPc.

Section 5. STS Features of F_{16}ZnPc in the Binary Molecular Superstructure

As mentioned in the main text, it should be noted that the ~1e occupation of F_{16}ZnPc that is predicted by COMSOL simulations poses an interesting complication when considering STS data. During STS data acquisition of the unoccupied molecular state of F_{16}ZnPc, electrons are tunneled into the molecule directly below the STM tip. For the scenario of the binary blend, the 1e occupation of the F_{16}ZnPc LUMO suggests that the molecular orbital is now situated near or directly at the substrate Fermi level. As a result, the localized single electron occupation of the LUMO leads to a splitting of its STS feature into a singly unoccupied molecular orbital (SUMO) and a singly occupied molecular orbital (SOMO) which are separated by the intra-orbital Coulomb repulsion.[12, 15-18] This, therefore, suggests that the positive STS spectrum feature that is observed on F_{16}ZnPc constituents in the mixed layer could potentially be SUMO which is derived from the molecular LUMO. In the case of the pure F_{16}ZnPc layer, though the coexistence of the charged and neutral molecules in similar systems have been directly approved by ultraviolet photoemission spectroscopy (UPS) and x-ray photoemission spectroscopy (XPS) measurements owing to the timescale of the photoemission process (~ 1 fs), probing of dynamically charged molecules by STS is rather complicated.[19-22] Due to the technique's lack of temporal resolution and the strong local electric field between the tip and sample that can perturb the initial charge state of the molecule directly underneath the tip, all molecules appear similar in the STS measurements. However their LUMO energy levels are still susceptible to the vacuum level shift induced by the interfacial charge transfer, which is in agreement with what we observed in the pure F_{16}ZnPc layer.[19]

Material	$\mathbf{a_1(nm)}$	$\mathbf{a_2(nm)}$	$\boldsymbol{\theta}$**(degrees)**	Moiré Location	LUMO (eV)
ZnPc	1.36 ± 0.04	1.37 ± 0.05	87.5 ± 1.9	Hill	0.68 ± 0.08
				Valley	0.90 ± 0.04
F_{16}ZnPc	1.49 ± 0.05	1.39 ± 0.05	79.9 ± 4.3	Hill	0.46 ± 0.11
				Valley	0.72 ± 0.09
Mixed Binary Blend	2.03 ± 0.04	1.94 ± 0.04	88.2 ± 1.8	ZnPc Hill	0.93 ± 0.03
				ZnPc Valley	1.36 ± 0.03
				F_{16}ZnPc Hill	0.23 ± 0.03
				F_{16}ZnPc Valley	0.42 ± 0.03

Table S1: Lattice parameters and averaged Gaussian-fit peak positions of the unoccupied density of state features in the STS spectra taken on the ZnPc overlayer, the F_{16}ZnPc overlayer and the binary molecular superstructure, respectively. Note that the F_{16}ZnPc unit cell refers to the $\alpha\alpha$-orientation unit cell (see illustration of the orientation in Fig. S1c). For the LUMO levels, error bars represent the standard deviation of the peak position from multiple data sets, with the modulation voltage used as the lower bound.

Section 6. COMSOL Simulation

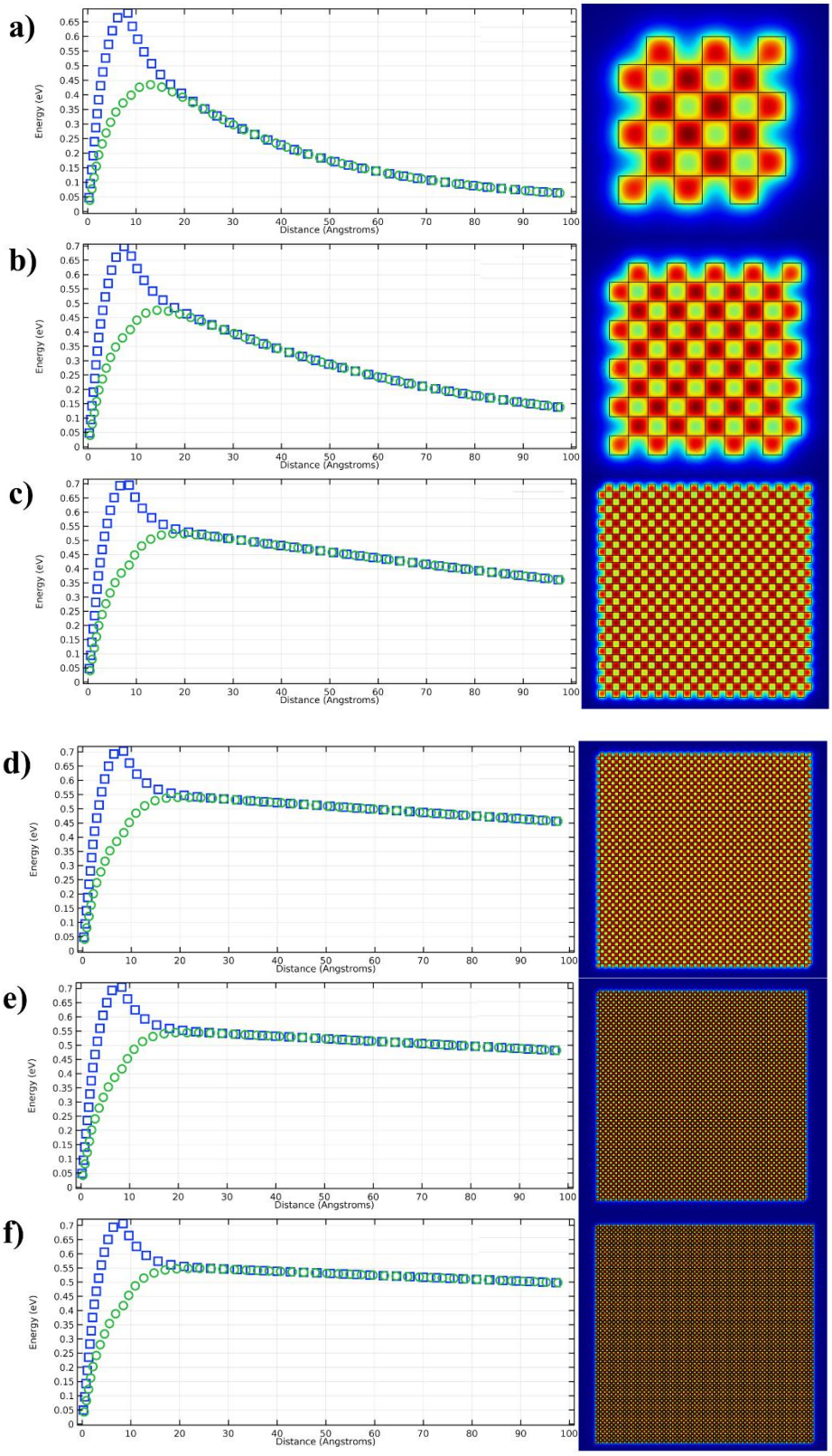

Figure S4: Finite element electrostatic simulation using COMSOL at (a) N=6, (b) N=10, (c) N=30, (d) N=60, (e) N=80, (f) N=100 molecules across, with the electrostatic potential energy for electrons plotted (left) from the image charge plane to 100 angstroms directly above ZnPc (green squares) and F_{16}ZnPc (blue squares) near the center of the binary molecular assembly. Right: Molecules are arranged in a N × N grid with each square representing a 1.44 nm × 1.44 nm Pc molecule, where the red areas are associated with fully charged F_{16}ZnPc molecules (1e per molecule) with higher electrostatic potential energy compared to the yellow areas of charge neutral ZnPc molecules. A maximum in the electrostatic potential energy can be seen directly above ZnPc, which represents the local vacuum level shift originating from the charge transfer between F_{16}ZnPc molecules and the underlying Cu substrate. While N is small, i.e., the radius of the molecular assembly is comparable to the distance from the molecular layer where the electrostatic potential energy for electrons is sought, small changes in the assembly size will lead to a sizable alteration in the potential energy. This probing distance, which is comparable to the position of the STM tip, is around 10-20 angstroms from the image charge plane of the Cu(111) substrate, corresponding to a tip-sample distance of under 1 nm. A change in the maximum potential energy, i.e., the local vacuum level shift, of about 0.1 eV can be observed when scaling from N=6 to N=60 and is stabilized for larger N's.

It is worth emphasizing that the discussion of a Madelung energy analog should strictly be treated as only an analog. A typical calculation of the Madelung energy involves treating the positive and negative charges of an ionic lattice as point charges with well-defined inter-charge distance. The Madelung energy contribution at site *i*, can be defined as: [23]

$$E_{M,i} = \frac{z_i e^2}{4\pi\epsilon_o} \cdot \sum_j \frac{z_j}{l_{ij}}$$

Where z_i and z_j are charges at the *i*th and *j*th site, respectively, while l_{ij} is the distance between the *i*th and *j*th sites. Applying this calculation to the mixed binary superstructure system can be quite challenging due to the substrate's image charge screening, both from the Cu and the dielectric spacer, h-BN, and their corresponding effects on the l_{ij} distance. Determination of a true Madelung energy for this system goes beyond the scope of this body of work.

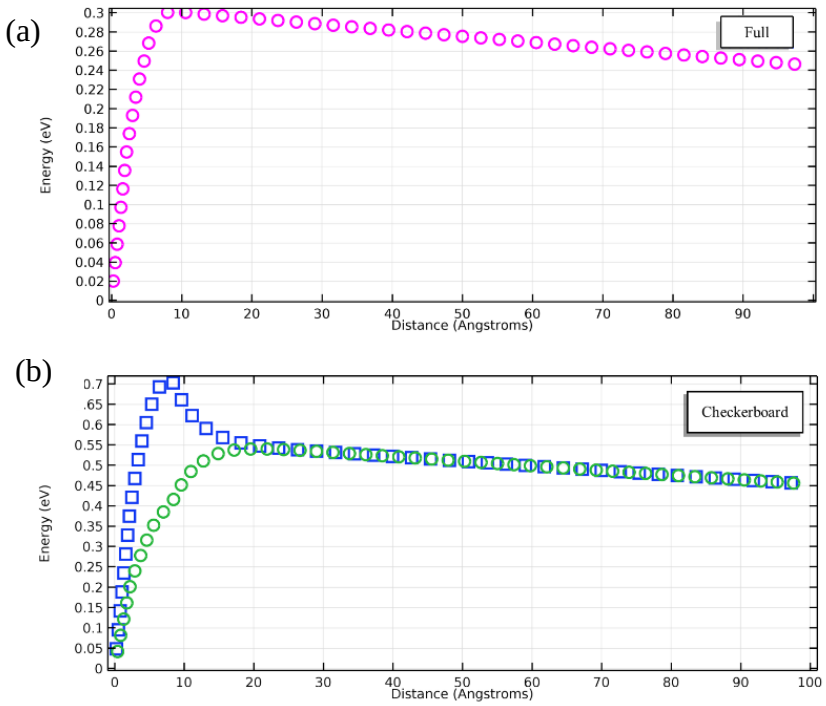

Figure S5: Finite element electrostatic simulation of the (a) pure F_{16}ZnPc and (b) mixed binary blend assemblies. 60 × 60 molecular matrix was used in both cases to calculate the electrostatic potential energy for electrons from the image charge plane of the metal substrate to 100 angstroms directly above the center of the molecular matrix in the pure layer (purple circles) in (a), and above ZnPc (green circles) and F_{16}ZnPc (blue squares) constituents near the center of the binary molecular assembly in (b). The potential energy for electrons reaches the maximum a couple of nanometers beyond the image charge plane, corresponding to the upshift of the local vacuum level. To establish the same magnitudes of the local vacuum level shifts as those extrapolated from the STS measurements (Fig. 2a in the manuscript), F_{16}ZnPc molecules in the pure layer are charged with 0.27e per molecule, while in the binary blend F_{16}ZnPc molecules are charged with 1e per molecule and ZnPc remain charge neutral.

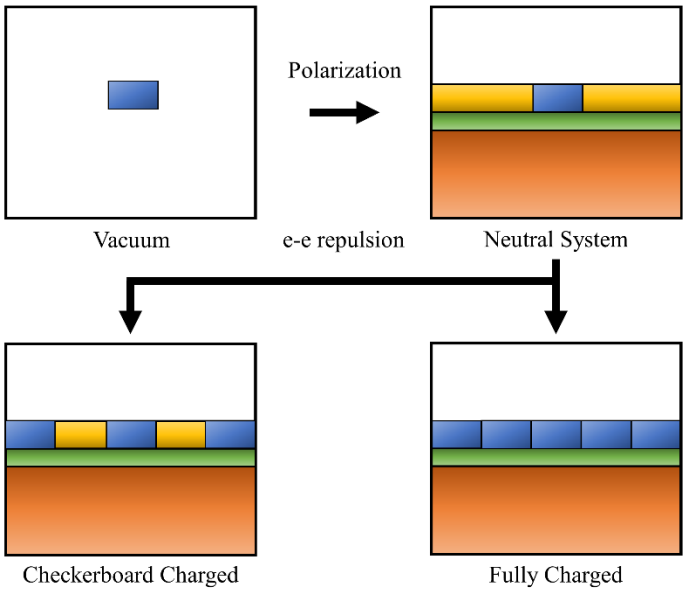

Figure S6: Schematic illustration of the different charging scenarios that result in the calculation of the Madelung energy for the pure $F_{16}ZnPc$ layer and the binary molecular superstructure. The polarization energy of 0.78 eV is determined by comparing the total electric potential energy of charging an organic molecule in vacuum vs. in a model system comprising of the Cu substrate, h-BN monolayer, and a continuous molecular dielectric layer. Since our COMSOL simulations assume a uniform charge density distribution, the total electric potential energy of charging an organic molecule can be calculated by using the simple equation of $E = \int \rho\Phi \, dV$ where ρ is the charge density in the molecule, Φ is the potential induced by the charge within the molecule. The e-e repulsion energy can be estimated in a matrix with the $F_{16}ZnPc$ molecules either charged in a checkerboard pattern mimicking the binary blend or on every molecular site for the pure layer. In comparison to the model system consisting of the continuum charge-neutral molecular dielectric layer, the additional electrostatic energy associated with charging a molecule in the charged matrix is, therefore, E_{ee}, which amounts to 0.07 eV for the checkerboard structure and 0.27 eV for the fully charged layer. Blue rectangles represent the charged $F_{16}ZnPc$ molecules, yellow areas are the continuous molecular dielectric layer comprised of neutral molecules, h-BN is denoted by the green area while Cu is the brown areas.

References

1. J. Q. Zhong, X. Qin, J. L. Zhang, S. Kera, N. Ueno, A. T. Wee, J. Yang and W. Chen, *ACS Nano*, 2014, **8**, 1699-1707.
2. Y.-L. Wang, J. Ren, C.-L. Song, Y.-P. Jiang, L.-L. Wang, K. He, X. Chen, J.-F. Jia, S. Meng, E. Kaxiras, Q.-K. Xue and X.-C. Ma, *Phys. Rev. B*, 2010, **82**, 245420.
3. Y. L. Huang, W. Chen, S. Chen and A. T. S. Wee, *Applied Physics A*, 2008, **95**, 107-111.
4. Y. Wakayama, *The Journal of Physical Chemistry C*, 2007, **111**, 2675-2678.
5. F. E. Olsson, M. Persson, A. G. Borisov, J. P. Gauyacq, J. Lagoute and S. Folsch, *Physical Review Letters*, 2004, **93**, 206803.
6. E. Zupanič, R. Žitko, H. Midden, I. Muševič and A. Prodan, *Croatica Chemica Acta*, 2009, **82**, 485–491.
7. O. I. Arillo-Flores, M. M. Fadlallah, C. Schuster, U. Eckern and A. H. Romero, *Physical Review B*, 2013, **87**, 165115.
8. F. C. Wu, H. L. Cheng, C. H. Yen, J. W. Lin, S. J. Liu, W. Y. Chou and F. C. Tang, *Phys Chem Chem Phys*, 2010, **12**, 2098-2106.
9. L. Liu, T. Dienel, R. Widmer and O. Groning, *ACS Nano*, 2015, **9**, 10125-10132.
10. R. Aroca, Z. Q. Zeng and J. Mink, *Journal of Physics and Chemistry of Solids*, 1990, **51**, 135-139.
11. I. Fernández Torrente, K. J. Franke and J. Ignacio Pascual, *Journal of Physics: Condensed Matter*, 2008, **20**, 184001.
12. K. A. Cochrane, A. Schiffrin, T. S. Roussy, M. Capsoni and S. A. Burke, *Nat Commun*, 2015, **6**, 8312.
13. K. A. Cochrane, T. S. Roussy, B. Yuan, G. Tom, E. Mårsell and S. A. Burke, *J Phys Chem C*, 2018, **122**, 8437-8444.
14. W. Tress, *Organic Solar Cells*, Springer2014.
15. O. T. Hofmann, P. Rinke, M. Scheffler and G. Heimel, *ACS Nano*, 2015, **9**, 5391-5404.
16. U. Ham and W. Ho, *J Chem Phys*, 2013, **138**, 074703.
17. J. Repp, G. Meyer, S. Paavilainen, F. E. Olsson and M. Persson, *Science*, 2006, **312**, 1196-1199.
18. M. Hollerer, D. Luftner, P. Hurdax, T. Ules, S. Soubatch, F. S. Tautz, G. Koller, P. Puschnig, M. Sterrer and M. G. Ramsey, *ACS Nano*, 2017, **11**, 6252-6260.
19. A. Della Pia, M. Riello, A. Floris, D. Stassen, T. S. Jones, D. Bonifazi, A. De Vita and G. Costantini, *ACS Nano*, 2014, **8**, 12356-12364.
20. P. Amsalem, J. Niederhausen, A. Wilke, G. Heimel, R. Schlesinger, S. Winkler, A. Vollmer, J. P. Rabe and N. Koch, *Phys. Rev. B*, 2013, **87**, 035440.
21. S. Winkler, P. Amsalem, J. Frisch, M. Oehzelt, G. Heimel and N. Koch, *Materials Horizons*, 2015, **2**, 427-433.
22. H. Wang, P. Amsalem, G. Heimel, I. Salzmann, N. Koch and M. Oehzelt, *Adv Mater*, 2014, **26**, 925-930.
23. L. Glasser, *Inorg Chem*, 2012, **51**, 2420-2424.